Maximum wind power plant generation by reducing the wake effect

Mikel De-Prada-Gil[a,*], César Guillén Alías[c], Oriol Gomis-Bellmunt[a,b,c], Andreas Sumper[a,b,c]

[a] *IREC Catalonia Institute for Energy Research, Jardins de les Dones de Negre 1, 2a. 08930 Sant Adrià de Besòs, Barcelona (Spain).*
[b] *Centre d'Innovació Tecnològica en Convertidors Estàtics i Accionaments (CITCEA-UPC), Universitat Politècnica de Catalunya UPC, C. Comte d'Urgell, 187, Pl. 2. 08036 Barcelona, Spain*
[c] *Centre d'Innovació Tecnològica en Convertidors Estàtics i Accionaments (CITCEA-UPC), Universitat Politècnica de Catalunya UPC, Av. Diagonal, 647, Pl. 2. 08028 Barcelona, Spain*

Abstract

This paper analyses, from a steady state point of view, the potential benefit of a Wind Power Plant (WPP) control strategy whose main objective is to maximise its total energy yield over its lifetime by taking into consideration that the wake effect within the WPP varies depending on the operation of each wind turbine. Unlike the conventional approach in which each wind turbine operation is optimised individually to maximise its own energy capture, the proposed control strategy aims to optimise the whole system by operating some wind turbines at sub–optimum points, so that the wake effect within the WPP is reduced and therefore the total power generation is maximised. The methodology used to assess the performance of both control approaches is presented and applied to two particular study cases. It contains a comprehensive wake model considering single, partial and multiple wake effects among turbines. The study also takes into account the Blade Element Momentum (BEM) theory to accurately compute both power and thrust coefficient of each wind turbine. The results suggest a good potential of the proposed concept, since an increase in the annual energy captured by the WPP from 1.86% up to 6.24% may be achieved (depending on

*Corresponding author
Email address: mdeprada@irec.cat. Jardins de les Dones de Negre 1, 2a. 08930 Sant Adrià de Besòs, Barcelona (Spain). Tel. +34 933562615 Fax. +34 933563802 (Mikel De-Prada-Gil)

the wind rose at the WPP location) by operating some specific wind turbines slightly away from their optimum point and reducing thus the wake effect.

Keywords: Wake effects, wind power generation, wind power plants (WPPs), wind turbine aerodynamics, wind turbine control

1. Introduction

Wind turbines interact with the wind, capturing part of its kinetic energy and converting it into electrical energy. Following directly on from the first principle of thermodynamics, this extraction of energy creates a wind energy deficit between the wind leaving the turbine (known as wake) and the wind arriving in front of the turbine. Thus, the wind speeds in the rear of the turbines are lower than the upstream wind speeds and, therefore, a reduction of power output is produced at downwind turbines. The turbine wake also causes high turbulence levels in downwind turbines, giving rise to additional mechanical stress, which may reduce their operating life [1, 2].

To date, Wind Power Plants (WPPs) seek to maximise their power generation by optimizing wind turbine performance individually while ensuring a safe operation by maintaining it within its admissible power and speed limits [3–6]. Besides, WPPs layouts are also optimised to minimise the wake effect [7]. This fact is especially relevant in offshore where wake effect is more significant than onshore where higher turbulence assists wind speed recovery [8]. Thus, wind turbines are typically spaced out by a certain distance resulting from a trade–off between maximising the WPP energy capture by reducing the wake effects and minimizing the costs associated with the logistics and electrical interconnections between turbines [9].

Recent studies have shown that operating each wind turbine at its optimal individual point without considering the impact of the wake effect on the other turbines does not maximise the power output of the whole wind power plant [10–16]. For this purpose, they suggest to increase the total WPP power generated and reduce structural loads by properly operating some wind turbines at non–

optimum points, based on the fact that operating the upstream turbines at a lower rotational speed results in higher wind speeds for downstream wind turbines. Accordingly, some publications develop optimisation algorithms based on heuristic methods [10, 13, 16] to maximise the total energy yield by the WPP, while others are focused on the operation and control of this new WPP concept [17, 18].

This paper proposes a new control strategy for this WPP concept based on a coordinated control between a centralised controller located in the offshore or onshore substation and local controllers installed on each turbine. This central controller optimises the operation of each wind turbine to maximise the total power output of the entire WPP, whilst the local controllers have the goal of regulating wind turbine speed to operate at such operation previously determined. Also, the paper carries out a comprehensive energy yield assessment for a WPP based on the proposed control strategy and compared to that obtained by using the conventional control approach. In order to perform a rigorous performance assessment in terms of energy capture, the aerodynamics principles of wind turbines are considered. The analysis methodology also includes a wake model considering single, partial and multiple wake effects among turbines within a WPP. With the aim to better understanding the proposed optimal WPP operation approach, first a very simple model consisting of three turbines aligned in a row is considered. Then, a more complex model based on a wind farm composed by 9 wind turbines (3×3 wind turbine array) is used to carry out an energy capture comparative analysis between both WPP control strategies. This study is performed taking into account two different wind roses to evaluate the influence of wind direction on the effectiveness of the proposed concept.

2. Wind turbine modelling

In this section, wind turbine is modelled according to the Blade Element Momentum (BEM) theory which is a combination of the momentum and blade element theory. This approach is used to analyse the aerodynamic of wind turbines characterised by their power (C_P) and thrust (C_T) coefficient. These

coefficients, especially C_T, are usually not provided for commercial turbines but are essential to quantify both the wind turbine rotor performance and the wind speed losses because of wake effects.

2.1. Blade element theory

The blade element theory defines the forces that act over the blade as a function of the lift (C_L) and drag (C_D) coefficients, which in turn depend on the angle of attack (α) [19]. As it is shown in Figure 1, the blade is assumed to be divided into N elements of width d_r and airfoil chord length c, at a distance r of the center.

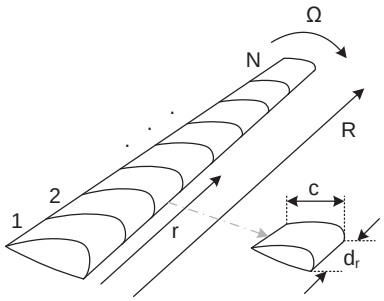

Figure 1: Schematic of blade divided into N elements of width d_r; c, airfoil chord length; r, radius; R, rotor radius; Ω, angular velocity of rotor.

Assuming that there is no aerodynamic interaction between elements, the following equations can be derived from Figure 2.

$$tan\varphi = \frac{U(1-a)}{r\Omega(1+a')} = \frac{1-a}{(1+a')\lambda_r} \quad (1)$$

$$U_{rel} = U(1-a)/sin\varphi \quad (2)$$

$$dF_L = C_L \frac{1}{2}\rho U_{rel}^2 c d_r \quad (3)$$

$$dF_D = C_D \frac{1}{2}\rho U_{rel}^2 c d_r \quad (4)$$

$$dF_N = dF_L cos\varphi + dF_D sin\varphi \quad (5)$$

$$dF_T = dF_L sin\varphi - dF_D cos\varphi \quad (6)$$

where ρ is the air density, U is the velocity of undisturbed air flow, a is the induction factor defined as the fractional decrease in wind velocity between the

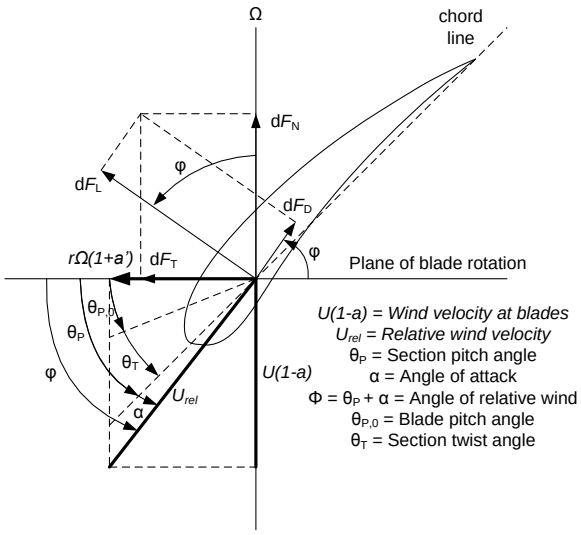

Figure 2: Blade section.

free stream and the rotor plane, Ω is the angular velocity of rotor, U_{rel} is the relative wind speed, $a' = \omega/2\Omega$ is the angular induction factor with ω being the angular velocity imparted to the flow stream and $\lambda_r = r\Omega/U$ is the ratio of the rotor speed at some intermediate radius to the wind speed (local speed ratio), which is related with the tip speed ratio as

$$\lambda_r = \lambda \frac{r}{R} \tag{7}$$

Likewise, dF_L is the incremental lift force, dF_D is the incremental drag force, dF_N is the incremental force normal to the plane of rotation and dF_T is the incremental force tangential to the circle swept by the rotor [19].

Combining from Eqs. (3) to (6) and considering a turbine with B blades, dF_N and dQ (torque differential) can be calculated as

$$dF_N = B\frac{1}{2}\rho U_{rel}^2 (C_L cos\varphi + C_D sin\varphi) c d_r \tag{8}$$

$$dQ = B r dF_T \quad \Longrightarrow \quad dQ = B\frac{1}{2}\rho U_{rel}^2 (C_L sin\varphi - C_D cos\varphi) c r dr \tag{9}$$

Hence, thrust and torque experienced by the turbine can be expressed as a function of the relative's wind angle, φ (that at constant pitch depends on the

angle of attack and the angular speed) and the lift and drag coefficients (also depending on the angle of attack).

2.2. Blade Element momentum theory

The Blade Element Momentum (BEM) theory combines the linear momentum theory (with wake rotation) and the blade element theory. This allows to compute the performance of a blade as a function of its design parameters and its operation, by assuming that the chord and the twist distributions of the blade are known [19].

BEM theory postulates that the forces and momentums over the blade must be equal by considering both theories. Thus, according to the momentum theory, the differential thrust (dT) and torque (dQ) are given by [19]

$$dT = \rho U^2 4a(1-a)\pi r dr \tag{10}$$

$$dQ = 4a'(1-a)\rho U \pi r^3 \Omega dr \tag{11}$$

whilst, from the blade element theory, the normal force (dF_N) and dQ are obtained as [19]

$$dF_N = \sigma' \pi \rho \frac{U^2(1-a)^2}{sin^2\varphi}(C_L cos\varphi + C_D sin\varphi) r dr \tag{12}$$

$$dQ = \sigma' \pi \rho \frac{U^2(1-a)^2}{sin^2\varphi}(C_L sin\varphi - C_D cos\varphi) r^2 dr \tag{13}$$

where dF_N is equivalent to dT, U_{rel} is substituted by Eq. (2) and σ' is the local solidity, defined by

$$\sigma' = \frac{Bc}{2\pi r} \tag{14}$$

Thus, combining the two theories according to the procedure explained in detail in [19], the power and thrust coefficients (C_P and C_T, respectively) can

be computed as

$$C_P = \frac{\int_{r_0}^{R} dP}{P_{tot}} = \frac{\int_{r_0}^{R} \Omega dQ}{\frac{1}{2}\rho\pi R^2 U^3} \tag{15}$$

$$C_{T,i} = \frac{dT}{dT_{tot}} = \frac{dF_N}{\frac{1}{2}\rho U^2 2\pi r dr} \tag{16}$$

which after some mathematical manipulations leads to the following expressions [20]

$$C_P = \frac{8}{\lambda^2}\int_{\lambda_h}^{\lambda} \lambda_r^3 a'(1-a)\left(1 - \frac{C_D}{C_L} cot\varphi\right) d\lambda_r \tag{17}$$

$$C_{T,i} = \frac{\sigma'(1-a_i)^2}{sin^2\varphi_i}(C_{l,i}cos\varphi_i + C_{d,i}sin\varphi_i) \tag{18}$$

Notice that according to the formulas above, C_P is for the whole turbine, while $C_{T,i}$ corresponds to the thrust coefficient of each one of the annular sections of the rotor, so that the C_T coefficient for the whole turbine would be the sum of all of them.

2.3. Tip losses

In order to compute C_P and C_T coefficients more accurately, the effect of the tip losses is included. These losses arise due to a pressure difference between the suction and pressure side of the blades giving rise to air flows around the tip from the lower to upper part, reducing lift and thus power at the last part of the blade.

The most straightforward way to compute this losses is by using the semi–empirical model developed by Prandtl [21], which takes into consideration the following correction factor F delimited between 0 and 1.

$$0 \leq F = \left(\frac{2}{\pi}\right) arccos\left[exp\left(-\frac{(B/2)\,(1-(r/R))}{(r/R)\,sin\varphi}\right)\right] \leq 1 \tag{19}$$

This correction factor affects the forces derived from the linear momentum

theory as follows

$$dT = F\rho U^2 4a(1-a)\pi r dr \tag{20}$$

$$dQ = F4a'(1-a)\rho U\pi r^3 \Omega dr \tag{21}$$

The rest of equations based on the blade element theory are based on the definition of forces acting over the blades and thus remain unchanged.

3. Wake effect modelling

Many comprehensive studies have been carried out regarding wind turbine wakes, and several models have been developed by researchers, such as Ainslie's model [22], Frandsen's model [23], Mosaic Tile model [24], Jensen's model [25] and CFD (Computational Fluid Dynamics) model [26]. The choice of the model depends on the desired prediction accuracy and on computational time. One of the most widely used wake model, developed by Jensen [25], is chosen for this study, as it provides adequate accuracy and reduced computational time [27]. It is based on global momentum conservation in the wake downstream of the wind turbine and assumes that the wake downstream of the turbine expands linearly.

In this paper, the wake model implemented takes into consideration the effect of single, partial and multiple wakes within a wind farm. Although all the equations used have been extensively reported in literature [25, 28–30], they are presented below for the sake of clarity.

- **Single wake:**

$$U_2 = U_1 \left[1 - \left(\frac{D}{D + 2 \cdot k_d \cdot x}\right)^2 (1 - \sqrt{1 - C_T})\right] \tag{22}$$

  where U_2 is the wind speed at distance x from the turbine, D is the diameter of the turbine rotor, U_1 is the free stream wind speed and k_d is the wake decay constant or opening angle which represents the effects of

atmospheric stability. Jensen experimentally found the value of k_d to be 0.075 for onshore applications and 0.04 for offshore applications. All these parameters are shown in Figure 3.

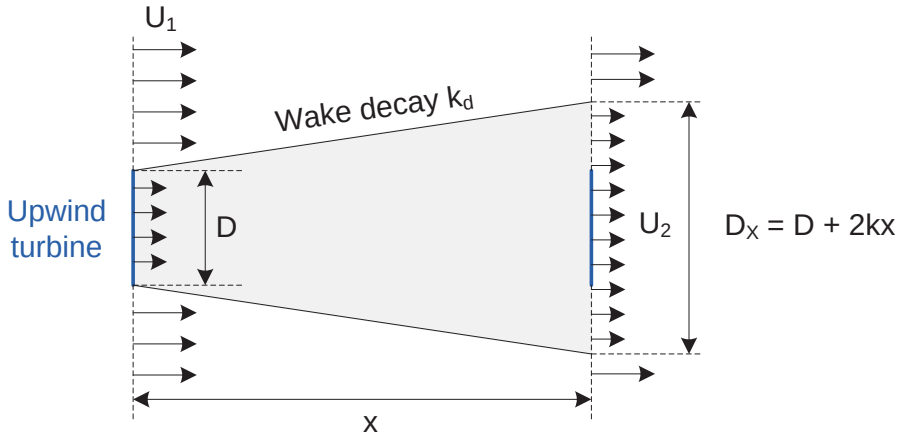

Figure 3: Schematic view of a single wake effect [25].

- **Partial wake:**

$$U_{Tj} = U_1 \left(1 - \sqrt{\sum_{k=1}^{N} \beta_{Tj,Tk} \left(1 - \frac{U_{ps,Tk}}{U_1}\right)^2}\right) \tag{23}$$

where U_{Tj} is the wind speed of the downwind turbine j, k is the upwind turbine, U_1 is the initial wind speed entering into the wind turbine k, $U_{ps,Tk}$ is the shadow of k falling on the j^{th} wind turbine, N is the number of wind turbines k that partially affect wind turbine j and $\beta_{Tj,Tk}$ is the ratio (the weighting factor) of the shadow area by the wake to the total rotor area (see Figure 4).

- **Multiple wakes:**

$$1 - \frac{U_x}{U_1} = \sqrt{\sum_{i=1}^{N} \left(1 - \frac{U_i}{U_1}\right)^2} \tag{24}$$

where U_1 is the initial free stream velocity, N is the total number of upwind influencing turbines, U_i is the wind speed affected by the individual wake

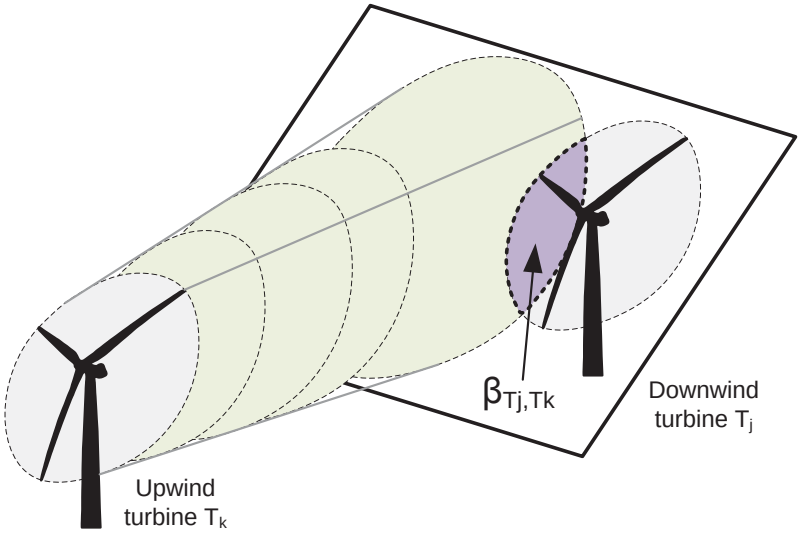

Figure 4: The shade area of a downstream wind turbine in partial wakes.

i and U_x is the wind speed such that all the wakes are taken into account. Figure 5 shows an illustrative example in which wind turbine 5 (wt_5) is affected by multiple wakes coming from wt_1, wt_2 and wt_4.

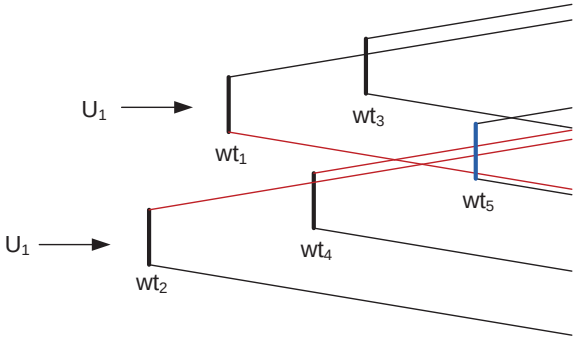

Figure 5: Illustrative example of multiple wakes in which wt_5 is affected by wt_1, wt_2 and wt_4.

4. Conceptual control structure

Figure 6 presents a conceptual scheme of the proposed control system. As it can be seen, unlike a conventional control system based on an individual

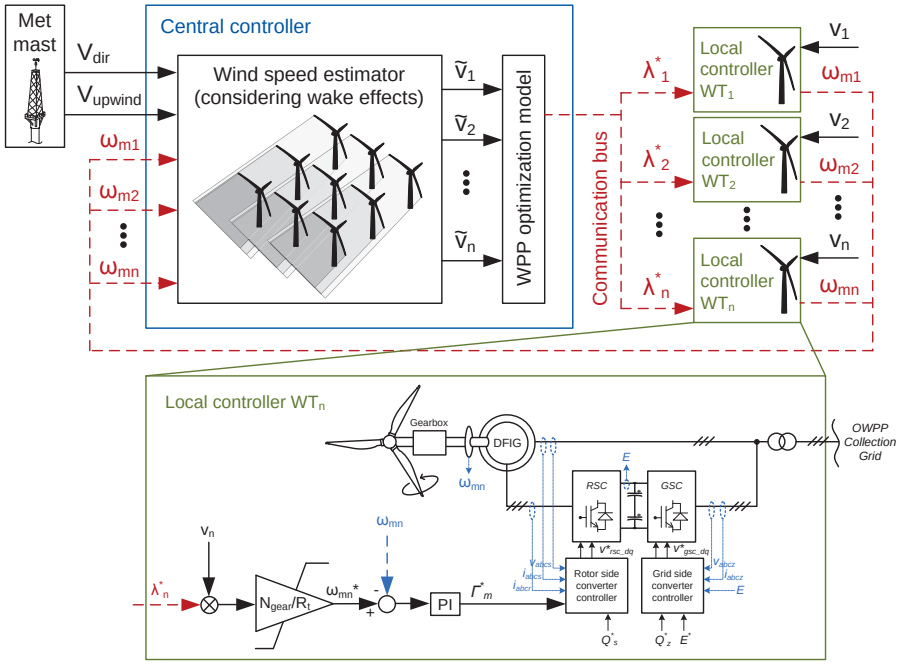

Figure 6: Scheme of the proposed control system.

control approach in which a MPPT algorithm is implemented in each wind turbine [4], this new control strategy proposes a coordinated control between wind turbines consisting of a centralised controller located in the offshore or onshore substation and local controllers installed on each turbine. The process is explained as follows:

- Wind speeds of each individual wind turbine are estimated according to different input data such as wind direction (V_{dir}) and free–stream wind speed (V_{upwind}) measured at one or several met masts installed around the WPP area, the rotational mechanical speed measurements of each turbine on the high speed shaft (ω_{mi}), as well as the WPP layout. These wind speed estimations, ($\tilde{v}_i$), are obtained taking into account the wake effect within the WPP (by considering single, partial and multiple wakes).

- Then, the centralised controller carries out an optimization process to

calculate the optimal tip speed ratios (λ_i^*) of each wind turbine that maximises the power output of the whole WPP. It is worth noting that these optimal set points may not be the same as those obtained by considering a MPPT approach.

- Finally, the local controller of each wind turbine regulates its rotational speed according to its optimal tip speed ratio previously computed. As it can be seen in Figure 6, this speed control compares the measured rotational speed of the generator (ω_m) to its reference signal (ω_m^*) to produce the reference electromagnetic torque (Γ_m^*) which is in turn regulated by the rotor side converter. It should be remarked that this control strategy is only applied for partial operation (below rated wind speed). Otherwise, in full load region, the torque reference signal is fixed whereas the pitch control is activated to limit the captured power to its nominal value.

5. Optimal wind power plant operation

As previously mentioned, this paper aims to analyse the potential benefits of applying the optimal WPP operation (which takes into consideration the wake effect within the WPP) in comparison to the conventional control strategy based on maximising the energy captured by the WPP by operating each turbine at its optimal individual point. Thus, the following analysis methodology has been developed and applied to two particular study cases to assess the performance of both control approaches.

5.1. Methodology description

A simple example is presented in order to facilitate the comprehension of the proposed methodology. The example aims to show that the total power generated by the WPP can be increased by properly operating some wind turbines at non–optimum points and, therefore allowing the downstream turbines to produce more power, rather than by using the conventional MPPT approach based on optimizing the operation of each wind turbine individually. As it can

be seen in Figure 7, it consists of three wind turbines aligned in a row with a rated power of 5 MW, a rotor diameter of 126 m and a rated wind speed of 11.2 m/s . The spacing between wind turbines is 7 rotor diameters (D).

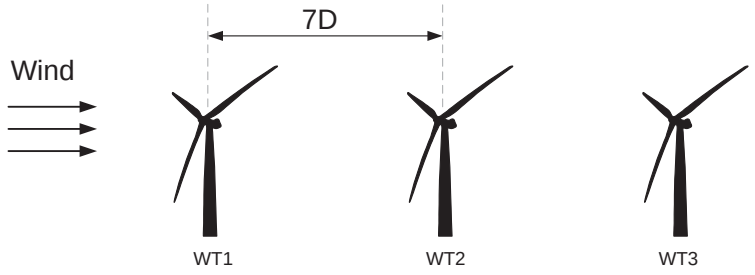

Figure 7: Schematic layout of the system under study consisting of three wind turbines aligned in a row.

The power coefficient (C_P) and thrust coefficient (C_T) curves used for the study are computed based on the BEM theory explained above by considering the specific NACA 4412 airfoil wind blade reported in [31]. The lift (C_L) and drag (C_D) coefficients are obtained according to an appropriate Reynolds number for the operating conditions. All these coefficients are depicted in Figure 8.

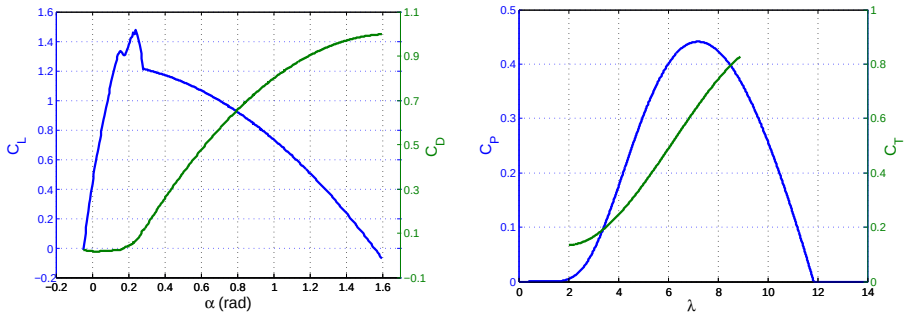

(a) (b)

Figure 8: (a) Lift (C_L) and drag (C_D) coefficients as a function of the angle of attack (α) on a NACA 4412 airfoil. (b) Power coefficient (C_P) and thrust coefficient (C_T) used for the study.

The procedure of obtaining the optimal operating points of each wind turbine

that maximise the total WPP power generation is described as follows:

- **Step 1:** Firstly, the power generated by the upstream wind turbines is calculated for all their operating points (i.e., varying their tip speed ratios, λ_1, from 2 to 9). For this particular example, only the power produced by WT1 is computed since it is assumed that the wind comes just from the one direction indicated in Figure 9. Thereby, the power generated by WT1 can be expressed as

$$P_{WT1}(\lambda_1) = \frac{1}{2}\rho A C_P(\lambda_1) U_1^3 \qquad \forall\ \lambda_1, \lambda_2 \in [2, 9] \tag{25}$$

  where U_1 is the upwind speed and the power coefficient, C_P, is only dependent on the tip speed ratio, λ_1, since the pitch angle, θ_{pitch}, is set to zero.

  Figure 9 presents the results obtained by computing Eq. (25). As it is shown, the optimal tip speed ratio (λ_1^*) that maximises the power output of WT1 $\left(\left.\frac{dP_{WT1}}{d\lambda_1}\right|_{\lambda_1^*} = 0\right)$ is $\lambda_1^* = 7.22$, regardless of the λ_2^* value.

- **Step 2:** Secondly, the power produced by the first turbines affected by the wake effect (in this case WT2) is computed according to the following equation

$$P_{WT2}(\lambda_1, \lambda_2) = \frac{1}{2}\rho A C_P(\lambda_2) U_2^3(\lambda_1) \qquad \forall\ \lambda_1, \lambda_2 \in [2, 9] \tag{26}$$

  As it can be seen, it depends on two parameters: λ_1 and λ_2. The former has an influence on wind speed of WT2 (U_2) by modifying the $C_T(\lambda_1)$ value (using Eq. (22)), whilst the latter changes the power coefficient of WT2 $C_P(\lambda_2)$ similarly to the previous case with WT1. Thus, the resulting surface $P_{WT2}(\lambda_1, \lambda_2)$ of computing Eq. (26) for all possible combinations of λ_1 and λ_2 parameters, is depicted in Figure 10.

  It should be noted that maximum power generation for WT2 is achieved when λ_1^* is minimum and $\lambda_2^* = 7.22$. This result is consistent with the

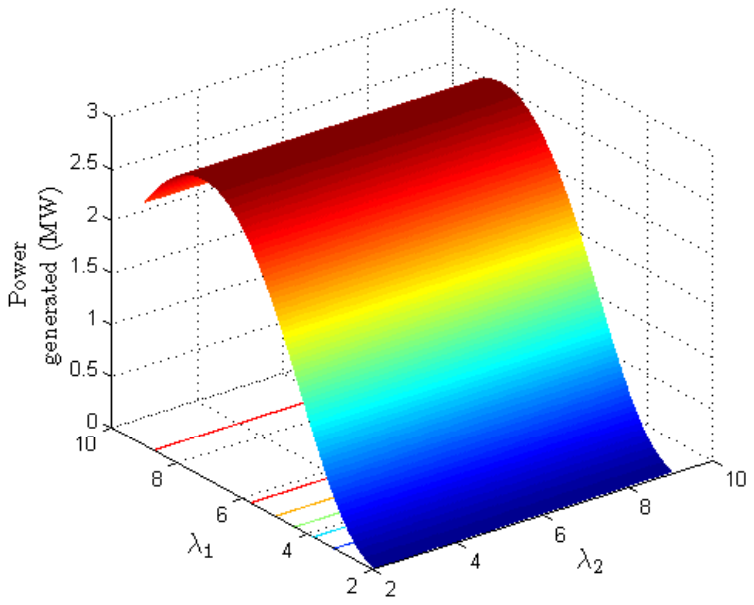

Figure 9: Power generated by the upwind turbine (WT1) as a function of λ_1 and λ_2. Upwind speed=9.5 m/s.

fact that the lower the rotational speed of WT1 (lower λ_1), the smaller the impact of the wake effect on downstream wind turbines and, therefore, the greater the power produced by WT2.

- **Step 3:** Next, the power extracted by those turbines whose wake do no affect other wind turbines (in this case WT3) are calculated as

$$P_{WT3}(\lambda_1, \lambda_2) = \frac{1}{2}\rho A C_P^{max} U_3^3(\lambda_1, \lambda_2) \qquad \forall\ \lambda_1, \lambda_2 \in [2, 9] \tag{27}$$

In this example, WT3 operates at its optimum point (C_P^{max}) because no downstream wind turbine is located behind. Regarding its wind speed (U_3), it is computed by considering the multiple wakes described in Eq. (24). Figure 11 shows the power P_{WT3} obtained by sweeping λ_1 and λ_2 from 2 to 9.

As expected, the maximum power that can be generated by WT3 occurs when the operating points of WT1 and WT2 are minimum.

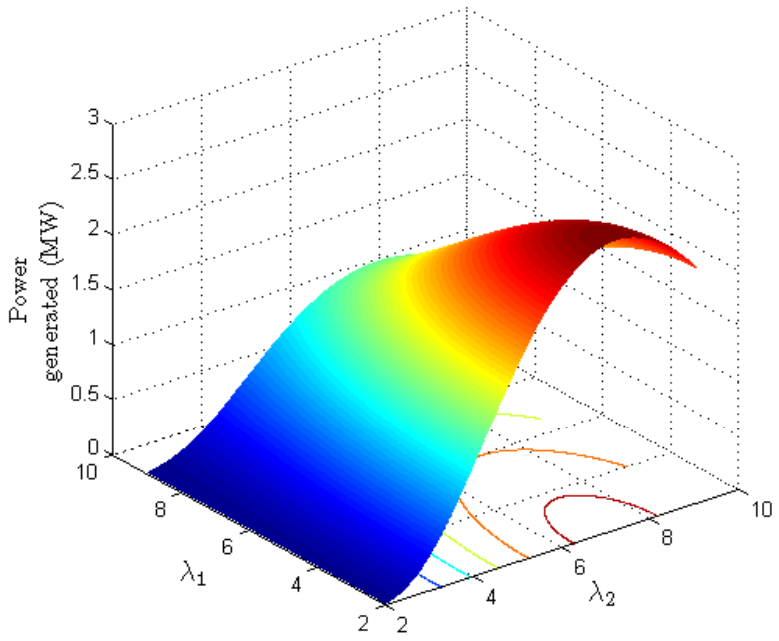

Figure 10: Power generated by WT2 as a function of λ_1 and λ_2. Upwind speed=9.5 m/s.

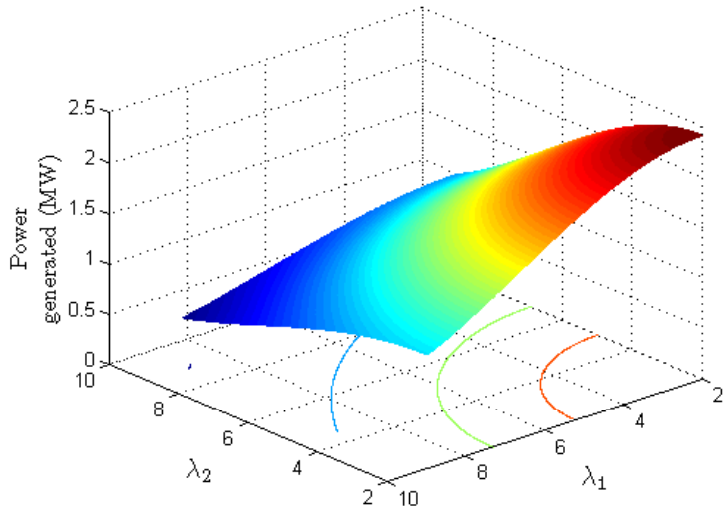

Figure 11: Power generated by WT3 as a function of λ_1 and λ_2. Upwind speed=9.5 m/s.

- **Step 4:** Finally, the total power produced by the set of the three wind turbines ($P_{TOT} = P_{WT1} + P_{WT2} + P_{WT3}$) is presented in Figure 12.

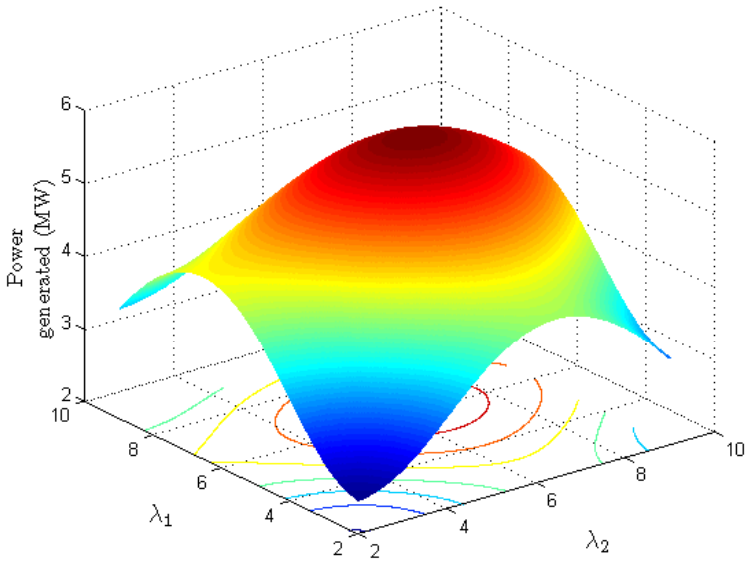

Figure 12: Total power generated by the set of three wind turbines (WT1, WT2 and WT3) as a function of λ_1 and λ_2. Upwind speed = 9.5 m/s.

As it can be seen, P_{TOT} reaches its maximum value for $\lambda_1^* = 6.12$ and $\lambda_2^* = 6.43$. It is worth noting that although the available data of tip speed ratio (λ) for the C_T curve are constrained within the range [2,9] (Figure 8), it does not pose a problem for the purpose of the study since the optimal operation points obtained for each turbine are within these boundaries.

Given the new tip speed ratios for each wind turbine, their new nominal operating points can be obtained, as it is shown in Table 1. In order to compare

Table 1: Nominal operating points of each wind turbine.

	λ^N	C_P^N	U_s^N (m/s)	ω^N (rad/s)
WT1	6.12	0.4075	11.7121	1.1377
WT2	6.43	0.4241	11.5574	1.1796
WT3	7.22	0.4412	11.4060	1.3072

the operation of each wind turbine for the two aforementioned control strategies analysed, Figure 13 is presented. It shows the tip speed ratio and power generated by each turbine as a function of the upwind speed. As it can be noted, WT2 and WT3 reach their rated power at higher wind speeds when the conventional WPP operation approach is applied because of the increased wake effect. Moreover, whereas the three wind turbines operate at their optimum point (λ_{opt}) by considering the conventional control strategy, the proposed WPP control method forces WT2 and WT3 to operate at sub–optimum points. It is worth remarking that the abscissa for all the graphs of Figure 13 refers to the upwind speed. Therefore, it is reasonable that the wind speeds from which WT2 and WT3 operate at their rated values are slightly higher than their nominal values shown in Table 1.

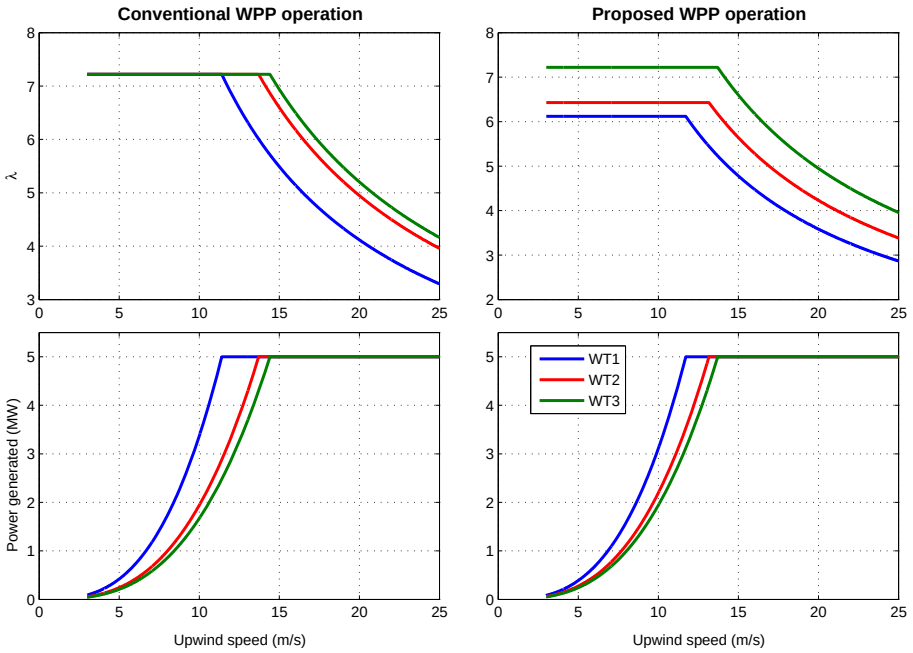

Figure 13: Tip speed ratio (λ) of each wind turbine (up) and power generated by each wind turbine (down) as a function of the upwind speed (considering wake effects) for both control strategies analysed.

To perform a technical assessment of both WPP control schemes (conventional and proposed WPP operation) the power generated and the energy yield per year by the set of three wind turbines (WT1, WT2 and WT3) as a function of the upwind speed is calculated and displayed in Figure 14. As it is shown, the effectiveness of operating the appropriate wind turbines at their non–optimum points to maximise the total energy capture by the WPP is demonstrated. Thus, the energy extracted per year by the set of three wind turbines is 44.62 GWh/year for the optimal WPP operation case and 42.85 GWh/year by considering the conventional approach based on optimal WT operation. It represents an increase of 3.97% of the energy produced per year.

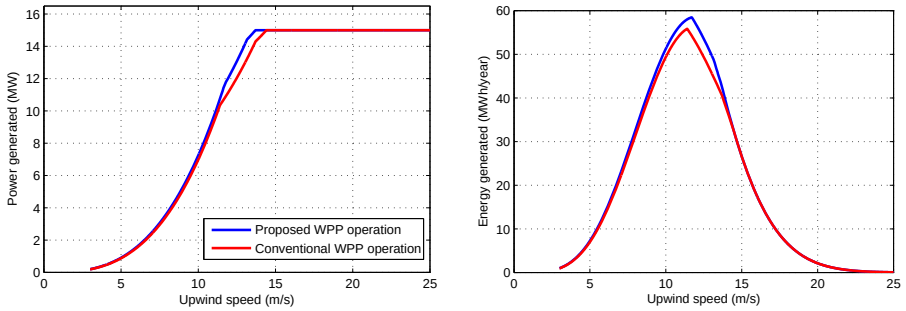

(a) (b)

Figure 14: Power produced (a) and energy yield (b) by the set of three wind turbines (WT1, WT2 and WT3) as a function of the upwind speed for both types of control systems.

It is important to note that the wind direction assumed for this conceptual case study is always kept constant (best possible scenario for the proposed concept). Thus, in order to accurately quantify both WPP operation alternatives, this methodology is applied to a realistic case study, in which the wind direction is changing with the time.

5.2. Application case

The wind power plant layout of the system under study is shown in Figure 15. It consists of 9 wind turbines laid out in a rectangular matrix of 3 rows and 3 columns. The spacing between wind turbines is detailed in the figure. Each

wind turbine has the same characteristics of the previous case, i.e., 5 MW of rated power, 126 m of rotor diameter and 11.2 m/s of rated wind speed.

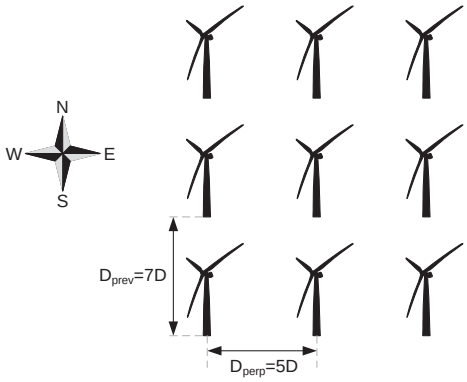

Figure 15: Schematic layout of the system under study consisting of 9 wind turbines laid out in a regular matrix of 3 rows and 3 columns.

Wind speed of each upstream turbine is randomly generated by means of a normal distribution function, $\mathcal{N}(\mu_i, \sigma_k^2)$, whose mean value μ is estimated by using a Weibull distribution function with the dimensionless shape (k) and scale (c) parameters obtained from [32, 33], and the standard deviation parameter σ is set to 0.5 m/s. It has been considered 12 incoming wind direction sectors of 30° each.

Figure 16 displays the wake effect within the wind farm for each wind direction sector considered in the study. As it can be seen, the impact of wake effect on the wind turbines can be classified into three main groups:

- for wind direction sectors of 0°, 90°, 180° and 270°, six wind turbines are completely affected by wakes (three affected by single wakes and three by multiple wakes).

- for wind direction sectors of 30°, 150°, 210° and 330°, four wind turbines are partially affected by wakes (three affected by partial wakes and one by multiple wakes).

- for wind direction sectors of 60°, 120°, 240° and 300°, only two wind

turbines are partially affected by wakes (both affected by partial wakes and none by multiple wakes).

Analogously to the previous case, the procedure of obtaining the optimal operating points of each wind turbine, for each wind direction sector, that maximise the total WPP power generation is carried out. Table 2 shows the obtained results. It should be noted that wind direction sectors of 0° and 180° are distinguished from 90° and 270° because of the spacing between wind turbines is different.

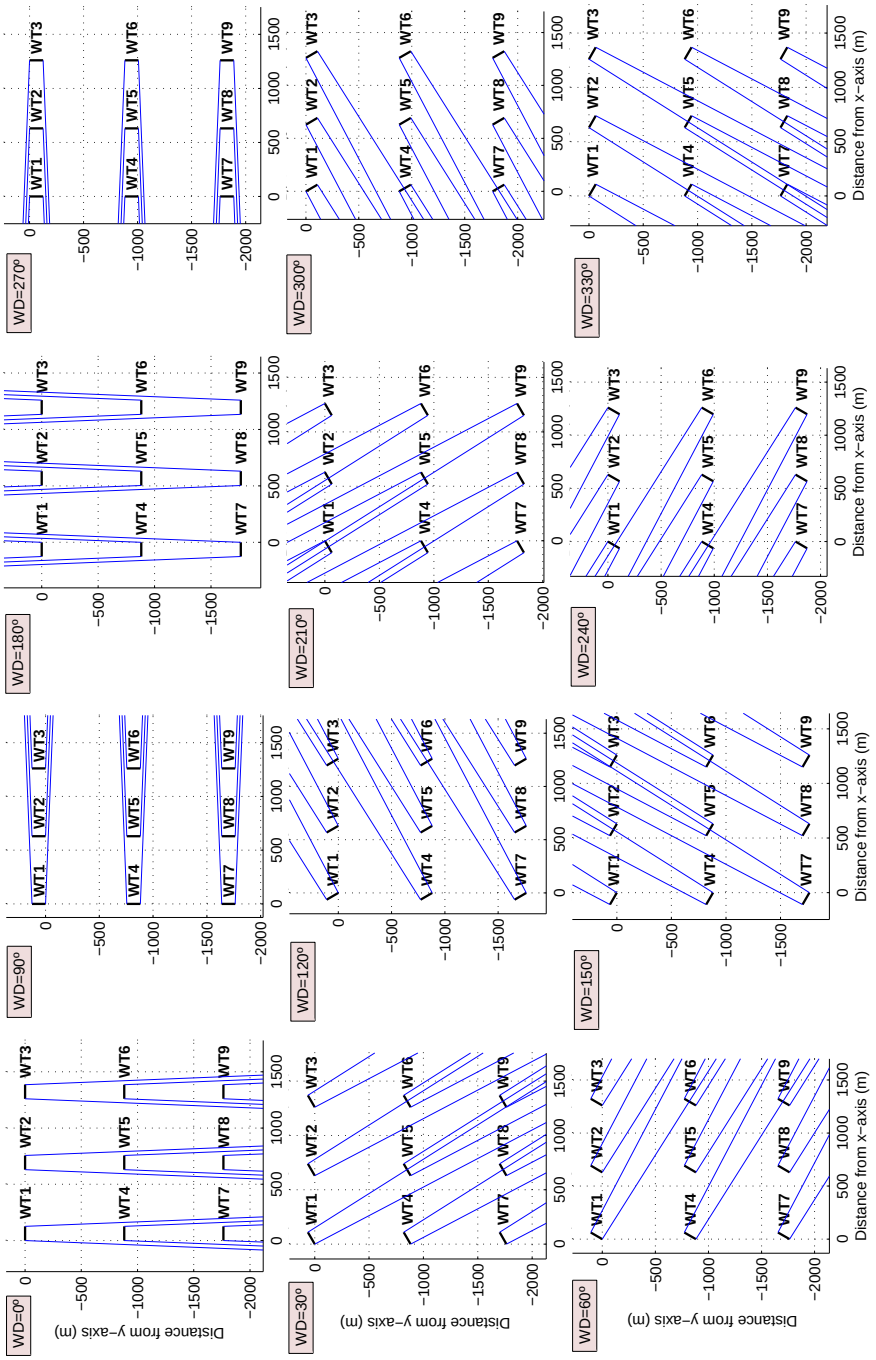

Figure 16: Wake effect within the wind farm for each wind direction sector considered in the study.

Table 2: Nominal operating points of all the wind turbines for any wind direction.

(a) Wind directions = 0° and 180°

	λ^N	C_P^N	U_s^N (m/s)	ω^N (rad/s)
Upwind turbines	6.12	0.4075	11.7121	1.1377
WTs affected by single wakes	6.43	0.4241	11.5574	1.1796
WTs affected by multiple wakes	7.22	0.4412	11.4060	1.3072

(b) Wind directions = 90° and 270°

	λ^N	C_P^N	U_s^N (m/s)	ω^N (rad/s)
Upwind turbines	6.01	0.4003	11.7820	1.1240
WTs affected by single wakes	6.30	0.4178	11.6150	1.1615
WTs affected by multiple wakes	7.22	0.4412	11.4060	1.3072

(c) Wind directions = 30°, 150°, 210° and 330°

	λ^N	C_P^N	U_s^N (m/s)	ω^N (rad/s)
Upwind turbines	6.62	0.4315	11.4910	1.2075
WTs affected by partial wakes	6.74	0.4351	11.4593	1.2260
WTs affected by multiple wakes	7.22	0.4412	11.4060	1.3072

(d) Wind directions = 60°, 120°, 240° and 300°

	λ^N	C_P^N	U_s^N (m/s)	ω^N (rad/s)
Upwind turbines	6.88	0.4382	11.4318	1.2484
WTs affected by partial wakes	7.22	0.4412	11.4060	1.3072
WTs affected by multiple wakes	–	–	–	–

Once the nominal operating points of all the wind turbines for any wind direction sector are known, the power generated by each wind turbine as a function of the upwind speed can be determined. As it is shown in Figure 17, the power curves of each turbine obtained for the incoming wind directions of 60°, 120°, 240° and 300° are more similar than for other wind directions, since the wake effect has a reduced impact on the turbines. However, those are more different for wind directions of 90° and 270° as a consequence of the greatest wake effect. Next, similarly to the prior example, the power generated by the WPP for each wind direction sector considered, is calculated and presented in Figure 18. As discussed above, the major benefit of operating some wind turbines at their non–optimum points is given for wind directions of 90° and 270°, while the improved efficiency achieved for wind directions of 60°, 120°, 240° and 300° is very limited, as expected.

Finally, the energy yield per year by the WPP, for both control strategies

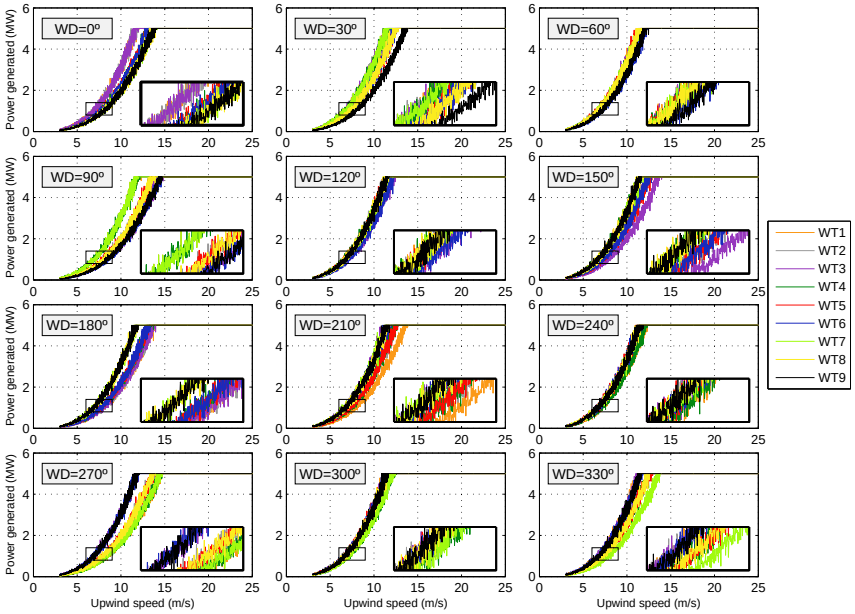

Figure 17: Power generated by each wind turbine, for each wind direction sector, as a function of the upwind turbine.

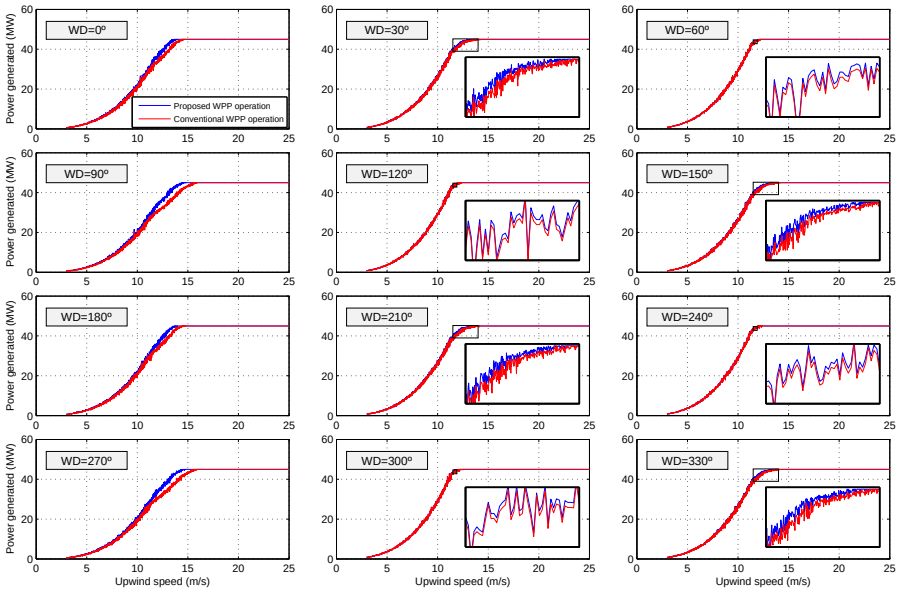

Figure 18: Power generated by the wind power plant (WPP), for each wind direction sector, as a function of the upwind turbine.

considered, is computed. In order to evaluate the influence of the probability of occurrence of the wind directions on the energy capture, two different wind roses distribution functions are taking into account. The results are presented in Figure 19 and detailed in Table 3.

Table 3: Technical assessment of both WPP control strategies considering two different wind roses.

	Energy yield (GWh/year)		**Energy increment**
	Scenario 1	**Scenario 2**	**(%)**
Wind rose (a)	117.89	125.74	6.24
Wind rose (c) [34]	142.37	145.07	1.86

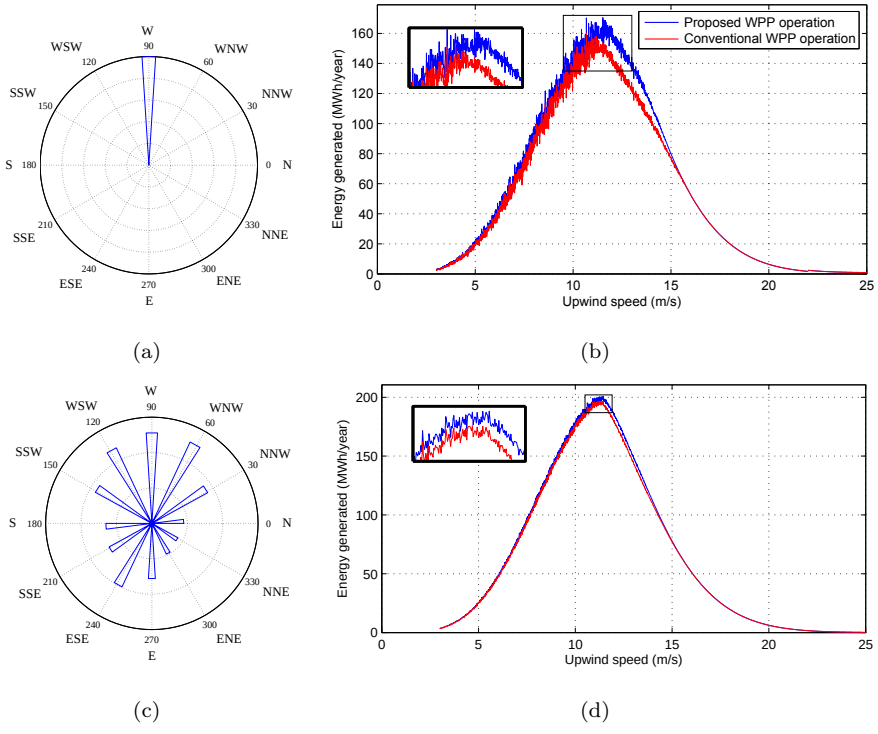

Figure 19: (a) and (c): Wind roses for the two cases under study. (b) and (d): Energy yield by the wind power plant (WPP) for both types of control systems and taking into account wind roses (a) and (c), respectively.

where scenario 1 refer to the proposed control strategy based on optimal WPP

operation and scenario 2 corresponds to the conventional approach based on optimal WT operation. The wind rose of Figure 19(c) is obtained from [34] and reports the meteorological mast data from Horns Rev.

Hence, the cost associated with the annual energy increment achieved during a lifetime of the installation of 20 years accounts for 5.75 M€ for wind rose (a) and 1.98 M€ for wind rose (c) considering a price of energy of 46.84 €/MWh [35], a market interest of 4.5% [36] and a rate of electricity price increase of 2% per year [37].

6. Conclusions

In this paper, the potential benefit of operating some wind turbines at their non–optimum points in the attempt of reducing the wake effect within a wind power plant, such that its total power output is maximised, is analysed from the steady state point of view. A description of the current wind power plant control strategy based on an individual optimisation of each turbine, as well as, the impact of wake effects on wind power generation, is presented. The implemented methodology has been applied to two particular study cases to assess the performance of both control approaches. According to the results obtained for both application examples, the effectiveness of the proposed concept is demonstrated. Thus, an increase from 1.86% up to 6.24% in the annual energy captured by the wind power plant can be achieved (depending on the wind rose at the WPP location) by operating the upstream turbines slightly away from their optimum point and reducing the wake effect within the wind power plant.

Acknowledgements

The research was supported by the EU under the FP7 project IRPWIND and by the Ministerio de Economía y Competitividad, Plan Nacional de I+D+i under Project ENE2012-33043.

[1] T. Ackermann, Wind Power in Power Systems, Wiley, 2005.

[2] F. D. Bianchi, H. D. Battista, R. J. Mantz, Wind Turbine Control Systems, Springer, 2007.

[3] W. M. Lin, C. M. Hong, F. S. Cheng, Design of intelligent controllers for wind generation system with sensorless maximum wind energy control, Energy Conversion and Management 52 (2) (2011) 1086–1096.

[4] R. Pena, J. C. Clare, G. M. Asher, Doubly fed induction generator using back-to-back PWM convertersand its application to variable-speed wind-energy generation, IEE Proceedings Electric Power Applications 143 (3) (1996) 231–241.

[5] Z. Lubosny, Wind Turbine Operation in Electric Power Systems, Springer, 2003.

[6] S. M. Muyeen, A. Al-Durra, J. Tamura, Variable speed wind turbine generator system with current controlled voltage source inverter, Energy Conversion and Management 52 (7) (2011) 2688–2694.

[7] Y. Chen, H. Li, K. Jin, Q. Song, Wind farm layout optimization using genetic algorithm with different hub height wind turbines, Energy Conversion and Management 70 (2013) 56–65.

[8] R. J. Barthelmie, S. C. Pryor, S. T. Frandsen, G. C. Larsen, Analytical modelling of large wind farm clusters, The science of making torque from wind, Copenhagen, Denmark, 2004, pp. 292–303.

[9] M. R. Mirghaed, R. Roshandel, Site specific optimization of wind turbines energy cost: Iterative approach, Energy Conversion and Management 73 (2013) 167–175.

[10] J. Serrano González, M. Burgos Payán, J. Riquelme Santos, Optimum Wind Turbines Operation for Minimizing Wake Effect Losses in Offshore Wind Farms, 13th International Conference on Environment and Electrical Engineering (EEEIC), Wroclaw, Poland, 2013.

[11] J. Annoni, P. Seiler, K. Johnson, P. Fleming, P. Gebraad, Evaluating Wake Models for Wind Farm Control, in: Accepted to the 2014 American Control Conference, 2014.

[12] C. G. Alías, Optimización de la generación de un parque eólico considerando efectos de estela, Master's thesis, UB-UPC dEnginyeria en Energia (June 2013).

[13] J. R. Marden, S. Ruben, L. Pao, A model-free approach to wind farm control using game theoretic methods, IEEE Transactions on Control Systems Technology (2013) 1207–1214.

[14] E. Bitar, P. Seiler, Coordinated control of a wind turbine array for power maximization, in: American Control Conference, Washington, DC, USA, 2013.

[15] K. E. Johnson, G. Fritsch, Assessment of extremum seeking control for wind farm energy production, Wind Engineering 36 (6) (2012) 701–716.

[16] P. M. O. Gebraad, F. C. van Dam, J. W. van Wingerden, A model-free distributed approach for wind plant control, in: American Control Conference, 2013, pp. 628–633.

[17] G. C. Larsen, H. A. Madsen, N. Troldborg, T. J. Larsen, P. E. Réthoré, P. Fuglsang, S. Ott, J. Mann, T. Buhl, M. Nielsen, TOPFARM-next generation design tool for optimisation of wind farm topology and operation, Tech. rep. (2011).

[18] D. Madjidian, A. Rantzer, A stationary turbine interaction model for control of wind farms, IFAC 18th World Congress, 2011.

[19] J. F. Manwell, J. G. McGowan, A. L. Rogers, Wind Energy Explained: theory, design and application, John Wiley and Sons, 2009.

[20] R. E. Wilson, P. B. S. Lissaman, Applied Aerodynamics of Wind Power Machine, 1974.

[21] O. D. Vries, Fluid Dynamic Aspects of Wind Energy Conversion, Tech. Rep. AGARD-AG-243, North Atlantic Treaty Organization (NATO). Advisory Group for Aerospace Research and Development (AGARD) (1979).

[22] J. F. Ainslie, Calculating the flowfield in the wake of wind turbines, Journal of Wind Engineering and Industrial Aerodynamics 27 (1988) 213 – 224.

[23] S. Frandsen, R. J. Barthelmie, S. C. Pryor, O. Rathmann, S. Larsen, J. Højstrup, M. Thøgersen, Analytical modelling of wind speed deficit in large offshore wind farms, Wind Energy 9 (1–2) (2006) 39–53.

[24] O. Rathmann, S. Frandsen, R. J. Barthelmie, Wake Modelling for intermediate and large wind farms, Wind Energy Conference & Exhibition (EWEC), Milan, Italy, 2007.

[25] N. O. Jensen, A note on wind generator interaction, Tech. rep., RISØ-M-2411, denmark (1983).

[26] P. E. Réthoré, A. Bechmann, N. Sørensen, S. T. Frandsen, J. Mann, H. E. Jørgensen, O. Rathmann, S. E. Larsen, A CFD model of the wake of an offshore wind farm: using a prescribed wake inflow, Journal of Physics: Conference Series 75 (1) (2007) 12–47.

[27] R. J. Barthelmie, L. Folkerts, G. C. Larsen, K. Rados, S. C. Pryor, S. T. Frandsen, B. Lange, G. Schepers, Comparison of Wake Model Simulations with Offshore Wind Turbine Wake Profiles Measured by Sodar, Journal of Atmospheric and Oceanic Technology 23 (2005) 888–901.

[28] M. De-Prada-Gil, O. Gomis-Bellmunt, A. Sumper, Technical and economic assessment of offshore wind power plants based on variable frequency operation of clusters with a single power converter, Applied Energy 125 (2014) 218–229.

[29] M. Ali, J. Matevosyan, J. V. Milanović, L. Söder, Effect of Wake Consideration on Estimated Cost of Wind Energy Curtailments, in: 8th International

Workshop on Large-Scale Integration of Wind Power into Power Systems as well as on Transmission Networks for Offshore Wind Farms, Bremen, Germany, 2009.

[30] M. De-Prada-Gil, O. Gomis-Bellmunt, A. Sumper, J. Bergas-Jané, Power generation efficiency analysis of offshore wind farms connected to a SLPC (single large power converter) operated with variable frequencies considering wake effects, Energy 37 (1) (2012) 455–468.

[31] NACA 4412 airfoil, http://airfoiltools.com/airfoil/details?airfoil=naca4412-il (Accessed on 16/04/2014).

[32] R. J. Barthelmie, S. C. Pryor, Can satellite sampling of offshore wind speeds realistically represent wind speed distributions?, Journal of Applied Meteorology 42 (1) (2003) 83–94.

[33] S. C. Pryor, M. Nielsen, R. J. Barthelmie, J. Mann, Can satellite sampling of offshore wind speeds realistically represent wind speed distributions? part ii: Quantifying uncertainties associated with distribution fitting methods, Journal of Applied Meteorology 43 (5) (2004) 739–750.

[34] C. B. Hasager, A. Pena, M. B. Christiansen, P. Astrup, M. Nielsen, F. Monaldo, D. Thompson, P. Nielsen, Remote Sensing Observation Used in Offshore Wind Energy, IEEE Journal of Selected Topics in Applied Earth Observations and Remote Sensing 1 (1) (2008) 67–79.

[35] Comisión Nacional de la Energía (CNE), Resultados del Mercado de Producción de Energía Eléctrica 2013, http://www.cne.es. (Accessed on 04/02/2014).

[36] European Central Bank (ECB), Money market interest rates, http://sdw.ecb.europa.eu (Accessed on 04/02/2014).

[37] Energy Information Administration (EIA), Annual Energy Outlook 2014, http://www.eia.gov/forecasts/aeo/er/index.cfm (Accessed on 04/02/2014).